Inorganic Chemistry
Article

Inorg. Chem. **2010**, *49*, 11403–11414 **11403**
DOI: 10.1021/ic1013335

Three-Dimensional Architectures Based on Lanthanide-Substituted Double-Keggin-Type Polyoxometalates and Lanthanide Cations or Lanthanide-Organic Complexes

Haiyan An,*,† Zhengbo Han,‡ and Tieqi Xu†

†*College of Chemistry, Dalian University of Technology, Dalian 116023, P.R. China, and*
‡*College of Chemistry, Liaoning University, Shenyang 110036, P.R. China.*

Received July 9, 2010

A family of three-dimensional (3D) architectures based on lanthanide-substituted polyoxometaloborate building blocks, $[LnK(H_2O)_{12}][Ln(H_2O)_6]_2[(H_2O)_4LnBW_{11}O_{39}H]_2\cdot 20H_2O$ (Ln = Ce **1**, Nd **2**), $H_2K_2(H_2O)_n[(C_6NO_2H_5)Ln(H_2O)_5]_2[(H_2O)_4LnBW_{11}O_{39}H]_2\cdot 18H_2O$ (Ln = Ce n = 8 **3**, Nd n = 9 **4**, $C_6NO_2H_5$ = pyridine-4-carboxylic acid), have been synthesized and characterized by elemental analysis, IR spectroscopy, thermogravimetric (TG) analysis, powder X-ray diffraction and single crystal X-ray diffraction. Compounds **1** and **2** are isostructural, and are built up of lanthanide-substituted double-Keggin-type polyoxoanions $[\{(H_2O)_4Ln(BW_{11}O_{39}H)\}_2]^{10-}$ linked by Ln^{3+} cations to form a 3D open framework with one-dimensional (1D) channels. The polyoxoanion $[\{(H_2O)_4Ln(BW_{11}O_{39}H)\}_2]^{10-}$ consists of two α_1-type mono-Ln-substituted Keggin anions, constituted by two $[BW_{11}O_{39}H]^{8-}$ polyoxoanions and two lanthanide cations. When pyridine-4-carboxylic acid ligand was added to the reaction system of **1**, **2**, compounds **3**, **4** were obtained. Isostructural compounds **3** and **4** are constructed from the lanthanide-substituted double-Keggin-type polyoxoanions $[\{(H_2O)_4Ln(BW_{11}O_{39}H)\}_2]^{10-}$ linked by the $[Ln(C_6NO_2H_5)]^{3+}$ bridges to form a 3D channel framework. From the topological point of view, the 3D nets of compounds **1**−**4** are binodal with three- and six-connected nodes and exhibit a rutile topology. Compounds **1**−**4** represent the examples of 3D architectures based on lanthanide-substituted polyoxometalates. The magnetic properties of compounds **1**−**4** have been studied by measuring their magnetic susceptibility in the temperature range 2−300 K.

Introduction

Polyoxometalates (POMs), as early transition metal oxide clusters, bear many properties that make them attractive for applications in catalysis, medicine, electronics, magnetism and optics.[1−3] An intriguing area in this field is the construction of three-dimensional (3D) framework materials based on POM building blocks and lanthanide cations or lanthanide-organic coordination complexes, not only from a structural point of view but also from the potential applications of these materials which range from gas adsorption, ion exchange, magnetism, and luminescence.[4] So far, the commonly used POM building blocks in this area still focus on the classic Anderson, Keggin, Silverton, and some isopolyoxoanion units,[4−6] owing to the great challenge of design and synthesis of new POM species. Recently, an effective strategy was developed to synthesize new POM species, that is, the use of vacant polyoxoanions as inorganic multidentate building blocks to "capture" transition metal or rare earth metal ions, leading to

*To whom correspondence should be addressed. Phone: +86-411-84706303. E-mail: anhy@dlut.edu.cn.

(1) (a) Pope, M. T. *Heteropoly and Isopoly Oxometalates*; Springer: Berlin, 1983. (b) Pope, M. T.; Müller, A. *Polyoxometalates: From Platonic Solids to Anti-Retroviral Activity*; Kluwer: Dordrecht, The Netherlands, 1993. (c) Pope, M. P.; Müller, A. *Polyoxometalate Chemistry: From Topology via Self-Assembly to Applications*; Kluwer: Dordrecht, The Netherlands, 2001. (d) Bösing, M.; Nöh, A.; Loose, I.; Krebs, B. *J. Am. Chem. Soc.* **1998**, *120*, 7252. (e) Soghomonian, V.; Chen, Q.; Haushalter, R. C.; Zubieta, J.; O'Connor, C. J. *Science* **1993**, *259*, 1596.
(2) (a) Hill, C. L. *Chem. Rev.* **1998**, *98*, 1. (b) Hou, Y.; Fang, X. K.; Hill, C. L. *Chem.—Eur. J.* **2007**, *13*, 9442. (c) Yamase, T.; Pope, M. T. *Polyoxometalate Chemistry for Nano-Composite Design*; Kluwer: Dordrecht, The Netherlands, 2002. (d) Fukaya, K.; Yamase, T. *Angew. Chem., Int. Ed.* **2003**, *42*, 654. (e) Mizuno, N.; Misono, M. *Chem. Rev.* **1998**, *98*, 199. (f) AlDamen, M. A.; Clemente-Juan, J. M.; Coronado, E.; Martí-Gastaldo, C.; Gaita-Arino, A. *J. Am. Chem. Soc.* **2008**, *130*, 8874. (g) Long, D. L.; Burkholder, E.; Cronin, L. *Chem. Soc. Rev.* **2007**, *36*, 105.
(3) (a) Tian, A. X.; Ying, J.; Peng, J.; Sha, J. Q.; Pang, H. J.; Zhang, P. P.; Chen, Y.; Zhu, M.; Su, Z. M. *Inorg. Chem.* **2009**, *48*, 100. (b) Zhang, J.; Hao, J.; Wei, Y. G.; Xiao, F. P.; Yin, P. C.; Wang, L. S. *J. Am. Chem. Soc.* **2010**, *132*, 14. (c) Lan, Y. Q.; Li, S. L.; Su, Z. M.; Shao, K. Z.; Ma, J. F.; Wang, X. L.; Wang, E. B. *Chem. Commun.* **2008**, 58. (d) Sun, C. Y.; Liu, S. X.; Liang, D. D.; Shao, K. Z.; Ren, Y. H.; Su, Z. M. *J. Am. Chem. Soc.* **2009**, *131*, 1883–1888. (e) Ibrahim, M.; Dickman, M. H.; Suchopar, A.; Kortz, U. *Inorg. Chem.* **2009**, *48*, 1649.
(4) Mialane, P.; Dolbecq, A.; Sécheresse, F. *Chem. Commun.* **2006**, 3477.
(5) (a) An, H. Y.; Xiao, D. R.; Wang, E. B.; Li, Y. G.; Wang, X. L.; Xu, L. *Eur. J. Inorg. Chem.* **2005**, 854. (b) An, H. Y.; Wang, E. B.; Xiao, D. R.; Li, Y. G.; Xu, L. *Inorg. Chem. Commun.* **2005**, *8*, 267.
(6) (a) Wu, C. D.; Lu, C. Z.; Zhuang, H. H.; Huang, J. S. *J. Am. Chem. Soc.* **2002**, *124*, 3836. (b) Izarova, N. V.; Sokolov, M. N.; Samsonenko, D. G.; Rothenberger, A.; Naumov, D. Y.; Fenske, D.; Fedin, V. P. *Eur. J. Inorg. Chem.* **2005**, 4985. (c) Zhang, X. T.; Wang, D. Q.; Dou, J. M.; Yan, S. S.; Yao, X. X.; Jiang, J. Z. *Inorg. Chem.* **2006**, *45*, 10629.

Published on Web 11/24/2010

diverse metal-substituted POMs with interesting properties.[7−10] In this aspect, lanthanide-substituted POMs (LSPs) built up of monovacant polyoxoanions and lanthanide cations have a larger volume and more negative charge than those of the commonly used POMs, which allow the formation of higher coordination numbers with metal cations, and may be excellent precursors to connect lanthanide cations or lanthanide-organic complex units to form charming 3D architectures.

Monovacant Keggin polyoxoanions $[SiW_{11}O_{39}]^{8-}$ and $[PW_{11}O_{39}]^{7-}$ with lanthanide cations can form discrete 1:1 and 1:2 type LSP clusters, studied by Peacock and Weakley et al. in 1971;[11] however, it was not until 2000 that Pope et al. first reported two infinite one-dimensional (1D) chains $[Ln(SiW_{11}O_{39})(H_2O)_3]^{5-}$ (Ln = La^{3+} and Ce^{3+}) constructed from 1:1 type LSPs coordinatively linked together by terminal oxygen atoms.[12] In 2003, Mialane et al. discovered another two inorganic 1D chains $[Yb(SiW_{11}O_{39})(H_2O)_2]^{5-}$ and $[Eu(SiW_{11}O_{39})(H_2O)_2]^{5-}$ based on 1:1 type LSPs, and a 2D layer structure $[Nd_2(SiW_{11}O_{39})(H_2O)_{11}]^{2-}$ based on 2:2 type LSPs.[13] Then, they isolated two 2:2-type hybrid LSPs $[\{(SiW_{11}O_{39})Ln(COOCH_3)(H_2O)\}_2]^{12-}$ (Ln = Gd^{3+} and Yb^{3+}).[14] In 2004, Nogueira et al. reported a novel discrete cluster $[Ce_2(PW_{10}O_{28})(PW_{11}O_{39})_2]^{17-}$, containing two monovacant $[PW_{11}O_{39}]^{7-}$ units and an unusual $[PW_{10}O_{28}]^{11-}$ unit linked by two Ce^{4+} ions.[15] Simultaneously, Francesconi et al. obtained a 1D polymer[16] $[Eu(H_2O)_4PW_{11}O_{39}]^{4-}$ similar to the $[Eu(SiW_{11}O_{39})(H_2O)_2]^{5-}$. Subsequently, Kortz et al. prepared a family of 1:2 type LSP clusters $[Ln(\beta_2\text{-}SiW_{11}O_{39})_2]^{13-}$ (Ln = La^{3+}, Ce^{3+}, Sm^{3+}, Eu^{3+}, Gd^{3+}, Tb^{3+}, Yb^{3+}, Lu^{3+})[17] based on monovacant precursor $[\beta_2\text{-}SiW_{11}O_{39}]^{8-}$. Since 2004, Niu's group successively synthesized some 1D chain and 2D layer derivatives based on 1:1 type LSPs ($[LnSiW_{11}O_{39}]^{5-}$ or $[LnGeW_{11}O_{39}]^{5-}$) and lanthanide cations or lanthanide-organic units such as, $[(Pr(H_2O)_4SiW_{11}O_{39})(NaPr_2(H_2O)_{12})(Pr(H_2O)_4SiW_{11}O_{39})]^{3-}$, $H\{[Sm(H_2O)_{5.5}(DMF)_{0.5}]_2[Sm(H_2O)_2(DMF)][Sm(H_2O)_3(\alpha\text{-}SiW_{11}O_{39})]_2\}$ and $[(CH_3)_4N]_2H_{1.50}[Nd_{1.50}(GeW_{11}O_{39})(H_2O)_6]$.[18] Recently, Niu et al. isolated two kinds of 2:2 type LSPs, $[\{(PW_{11}O_{39}H)Ln(H_2O)_3\}_2]^{6-}$ (Ln = Nd^{3+} and Gd^{3+}) and $[\{(PW_{11}O_{39})Ln(H_2O)(\eta^2,\mu\text{-}1,1)\text{-}CH_3COO\}_2]^{10-}$ [Ln = Sm^{3+}, Eu^{3+}, Gd^{3+}, Tb^{3+}, Ho^{3+}, Er^{3+}].[19] However, until now no 3D architectures based on LSPs have been reported. Therefore, it is quite appealing and challenging to search for suitable starting materials and reaction conditions to acquire 3D architectures based on LSPs and lanthanide linkers.

Interestingly, compared with plentiful researches on assemblies of lanthanide-substituted polyoxometalosilicates, germanates, or phosphates, the study on lanthanide-substituted polyoxometaloborates is very rare. To date only two structures based on polyoxometaloborates and lanthanide units determined by X-ray single-crystal diffraction are known, one is an isolated cluster $K_{8.5}H_{3.5}[Eu(BW_{11}O_{39})(W_5O_{18})]\cdot 25H_2O$,[20] and the other is a 1D chain $H_2(NH_4)_{10}[Ce_2(BW_{11}O_{39})_2(H_2O)_6]\cdot 21H_2O$.[21] Such cases show the difficulty in obtaining the single crystal of high quality for polyoxometaloborate-based compounds. We are interested in the synthesis and structural characterization of 3D complexes containing lanthanide units and vacant polyoxotungstoborates, and their applications. In this work, we choose monovacant Keggin $[BW_{11}O_{39}H]^{8-}$ as the precursor and study the interactions between the cluster and different lanthanide cations. Fortunately, we obtained two lanthanide-substituted polyoxotungstoborate-based compounds with 3D framework: $[LnK(H_2O)_{12}][Ln(H_2O)_6]_2[(H_2O)_4LnBW_{11}O_{39}H]_2\cdot 20H_2O$ (Ln = Ce **1**, Nd **2**). When pyridine-4-carboxylic acid molecule was introduced to the reaction system of **1** and **2**, we found that the organic ligand can effectively substitute the coordinated water molecule to form two lanthanide-substituted polyoxotungstoborate-based 3D hybrid compounds: $H_2K_2(H_2O)_n[(C_6NO_2H_5)Ln(H_2O)_5]_2[(H_2O)_4LnBW_{11}O_{39}H]_2\cdot 18H_2O$ (Ln = Ce $n = 8$ **3**, Nd $n = 9$ **4**). Compounds **1** and **2** are isostructural, and compounds **3** and **4** are also isostructural. They all possess a 3D framework and are built up of the 2:2 type lanthanide-substituted double-Keggin-type polyoxoanion $[\{(H_2O)_4Ln(BW_{11}O_{39}H)\}_2]^{10-}$ that consists of two α_1-type mono-Ln-substituted Keggin anions, prepared in situ. In compounds **1** and **2**, the $[\{(H_2O)_4Ln(BW_{11}O_{39}H)\}_2]^{10-}$ polyoxoanions are linked up together by Ln^{3+} cations to yield a 3D architecture with 1D channels. In compounds **3** and **4**, the $[\{(H_2O)_4Ln(BW_{11}O_{39}H)\}_2]^{10-}$ polyoxoanions are linked up together by Ln-pyridine-4-carboxylic acid units to yield a 3D framework with 1D channels. To our best knowledge, compounds **1**−**4** represent the first examples of 3D architectures based on LSPs. Furthermore, magnetic properties of compounds **1**−**4** have been investigated in the temperature range of 2−300 K.

Experimental Section

Materials and Measurements. $Ce(NO_3)_3\cdot 6H_2O$ and $Nd(NO_3)_3\cdot 6H_2O$ were commercially purchased. $K_8[BW_{11}O_{39}H]\cdot 13H_2O$ was synthesized according to the literature and characterized by IR spectroscopy.[22] All the other chemicals were commercially purchased and used without further purification. Elemental analyses (C, H, and N) were performed on a

(7) (a) Li, Y. W.; Li, Y. G.; Wang, Y. H.; Feng, X. J.; Lu, Y.; Wang, E. B. *Inorg. Chem.* **2009**, *48*, 6452. (b) Yao, S.; Zhang, Z. M.; Li, Y. G.; Wang, E. B. *Dalton Trans.* **2009**, 1786. (c) Zhang, Z. M.; Li, Y. G.; Wang, Y. H.; Qi, Y. F.; Wang, E. B. *Inorg. Chem.* **2008**, *47*, 7615.
(8) (a) Dolbecq, A.; Compain, J. D.; Mialane, P.; Marrot, J.; Rivière, E.; Sécheresse, F. *Inorg. Chem.* **2009**, *48*, 6452. (b) Wang, G. W.; Pan, C. L.; Li, K. C.; Cui, X. B.; Wang, H. T.; Wang, Y.; Shi, S. Y.; Xu, J. Q. *Inorg. Chem. Commun.* **2010**, *137*, 116. (c) Liu, H.; Qin, C.; Wei, Y. G.; Xu, L.; Gao, G. G.; Li, F. Y.; Qu, X. S. *Inorg. Chem.* **2008**, *47*, 4166.
(9) (a) Zheng, S. T.; Zhang, J.; Yang, G. Y. *Angew. Chem., Int. Ed.* **2008**, *47*, 3909. (b) Zhao, J. W.; Jia, H. P.; Zhang, J.; Zheng, S. T.; Yang, G. Y. *Chem.—Eur. J.* **2007**, 10030.
(10) Lu, Y.; Xu, Y.; Li, Y. G.; Wang, E. B.; Xu, X. X.; Ma, Y. *Inorg. Chem.* **2006**, *45*, 2055.
(11) Peacock, R. D.; Weakley, T. J. R. *J. Chem. Soc. A* **1971**, 1836.
(12) Sadakane, M.; Dickman, M. H.; Pope, M. T. *Angew. Chem., Int. Ed.* **2000**, *39*, 2914.
(13) Mialane, P.; Lisnard, L.; Mallard, A.; Marrot, J.; Antic-Fidancev, E.; Aschehoug, P.; Vivien, D.; Sécheresse, F. *Inorg. Chem.* **2003**, *42*, 2102.
(14) Mialane, P.; Dolbecq, A.; Rivière, E.; Marrot, J.; Sécheresse, F. *Eur. J. Inorg. Chem.* **2004**, 33.
(15) Sousa, F. L.; Paz, F. A. A.; Cavaleiro, A. M. V.; Klinowski, J.; Nogueira, H. I. S. *Chem. Commun.* **2004**, 2656.
(16) Zhang, C.; Howell, R. C.; Scotland, K. B.; Perez, F. G.; Todaro, L.; Francesconi, L. C. *Inorg. Chem.* **2004**, *43*, 7691.
(17) Bassil, B. S.; Dickman, M. H.; von der Kammer, B.; Kortz, U. *Inorg. Chem.* **2007**, *46*, 2452.
(18) (a) Wang, J. P.; Zhao, J. W.; Duan, X. Y.; Niu, J. Y. *Cryst. Growth Des.* **2006**, *6*, 507. (b) Niu, J. Y.; Zhao, J. W.; Wang, J. P. *Inorg. Chem. Commun.* **2004**, *7*, 876. (c) Wang, J. P.; Duan, X. Y.; Du, X. D.; Niu, J. Y. *Cryst. Growth Des.* **2006**, *6*, 2266.
(19) Niu, J. Y.; Wang, K. H.; Chen, H. N.; Zhao, J. W.; Ma, P. T.; Wang, J. P.; Li, M. X.; Bai, Y.; Dang, D. B. *Cryst. Growth Des.* **2009**, *9*, 4362.
(20) Naruke, H.; Yamase, T. *Bull. Chem. Soc. Jpn.* **2000**, *73*, 375.
(21) Sousa, F. L.; Paz, F. A. A.; Granadeiro, C. M. C. E.; Cavaleiro, A. M. V.; Rocha, J.; Klinowski, J.; Nogueira, H. I. S. *Inorg. Chem. Commun.* **2005**, *8*, 924.
(22) Tézé, A.; Michelon, M.; Hervé, G. *Inorg. Chem.* **1997**, *36*, 506.

Perkin-Elmer 2400 CHN elemental analyzer; B, K, W, Ce, Nd, Sm, and Eu were analyzed on a PLASMA-SPEC(I) ICP atomic emission spectrometer. IR spectra were recorded in the range 400−4000 cm^{-1} on an Alpha Centaur FT/IR Spectrophotometer using KBr pellets. Thermogravimetric (TG) analyses were performed on a Perkin-Elmer TGA7 instrument in flowing N_2 with a heating rate of 10 °C·min^{-1}. Powder X-ray diffraction (PXRD) data were collected with Cu Kα (λ = 1.542 Å) radiation on a Rigaku D/Max-2500 X-ray diffractometer. Variable-temperature magnetic susceptibility data were obtained on a SQUID magnetometer (Quantum Design, MPMS-7) in the temperature range 2−300 K with an applied field of 1 KOe. Corrections were applied for diamagnetism using Pascal's constants. Photoluminescence spectra were measured using a RF-5301-PC instrument (Japan) with 150 W xenon lamp.

Synthesis of $[LnK(H_2O)_{12}][Ln(H_2O)_6]_2[(H_2O)_4LnBW_{11}O_{39}H]_2\cdot 20H_2O$ (Ln = Ce 1, Nd 2). In a typical synthesis procedure for **1**, $Ce(NO_3)_3\cdot 6H_2O$ (0.868 g, 2 mmol) were dissolved in 20 mL of water. Then 40 mL water solution of $K_8[BW_{11}O_{39}H]\cdot 13H_2O$ (1.602 g, 0.5 mmol) was added to the above solution. The pH value of the mixture was adjusted to 3.5 using 1 mol L^{-1} NaOH under stirring, and the solution was refluxed for 2 h at 80 °C. The filtrate was kept for one month at ambient conditions, and then yellow diamondoid crystals of compound **1** were isolated in about 40% yield (based on Ce). Elemental analyses: Calcd for **1**: W, 57.84; Ce, 10.02; K, 0.56; B, 0.31; H, 1.52 (%). Found: W, 57.63; Ce, 10.12; K, 0.76; B, 0.41; H, 1.35(%). FTIR data (cm^{-1}): 3418(s), 1628(m), 1253(w), 998(m), 946(s), 850(vs), 790(s), 707(s) and 523(m).

The preparation of **2** was similar to that of **1** except that $Nd(NO_3)_3\cdot 6H_2O$ was used instead of $Ce(NO_3)_3\cdot 6H_2O$. Crystals of compound **2** were obtained in about 35% yield, respectively. Elemental analyses: Calcd for **2**: W, 57.67; Nd, 10.28; K, 0.56; B, 0.31; H, 1.51 (%). Found: W, 57.56; Nd, 10.40; K, 0.68; B, 0.43; H, 1.40 (%). **2**. FTIR data (cm^{-1}): 3400(s), 1627(m), 1255(w), 998(m), 947(s), 852(vs), 793(s), 707(s) and 523(m).

Synthesis of $H_2K_2(H_2O)_n[(C_6NO_2H_5)Ln(H_2O)_5]_2[(H_2O)_4LnBW_{11}O_{39}H]_2\cdot 18H_2O$ (Ln = Ce n = 8 3, Nd n = 9 4). In a typical synthesis procedure for **3**, pyridine-4-carboxylic acid (0.123 g, 1 mmol) and $Ce(NO_3)_3\cdot 6H_2O$ (0.868 g, 2 mmol) were orderly dissolved in 20 mL of water. Then a 40 mL water solution of $K_8[BW_{11}O_{39}H]\cdot 13H_2O$ (1.602 g, 0.5 mmol) was added to the above solution. The pH value of the mixture was adjusted to 3.5 using 1 mol L^{-1} NaOH under stirring, and the solution was refluxed for 2 h at 80 °C. The filtrate was kept for three weeks at ambient conditions, and then yellow diamondoid crystals of compound **3** were isolated in about 28% yield (based on Ce). Elemental analyses: Calcd for **3**: W, 57.81; Ce, 8.01; K, 1.12; B, 0.31; C, 2.06; H, 1.46; N, 0.40 (%). Found: W, 57.68; Ce, 8.22; K, 1.01; B, 0.44; C, 2.31; H, 1.32; N, 0.63 (%). FTIR data (cm^{-1}): 3418(m), 2923(w), 1622(m), 1600(m), 1397(m), 1252(w), 997(m), 946(s), 851(vs), 792(s), 708(s) and 522(m).

The preparation of **4** was similar to that of **3** except that $Nd(NO_3)_3\cdot 6H_2O$, was used instead of $Ce(NO_3)_3\cdot 6H_2O$. Crystals of compound **4** were obtained in about 40% yield. Elemental analyses: Calcd for **4**: W, 57.53; Nd, 8.21; K, 1.11; B, 0.31; C, 2.05; H, 1.48; N, 0.40 (%). Found: W, 57.39; Nd, 8.41; K, 1.02; B, 0.40; C, 2.35; H, 1.28; N, 0.60 (%). **4**. FTIR data (cm^{-1}): 3416(m), 1623(m), 1599(m), 1398(m), 1253(w), 997(m), 947(s), 854(vs), 793(s), 702(s) and 522(m).

Synthesis of $(C_6NO_2H_5)H_2K_2[(C_6NO_2H_5)_4Ln(H_2O)_2]_2[BW_{12}O_{40}]_2\cdot 12H_2O$ (Ln = Eu 5, Sm 6). The preparations of **5** and **6** were similar to that of **3** except that $Eu(NO_3)_3$ and $Sm(NO_3)_3$, were used instead of $Ce(NO_3)_3\cdot 6H_2O$. $Sm(NO_3)_3$ and $Eu(NO_3)_3$ were prepared by dissolving their oxides in dilute nitric acid and then heated to dryness. Crystals of compounds **5** and **6** were obtained in about 25, 27% yield, respectively. Elemental analyses: Calcd for **5**: W, 58.87; Eu, 4.05; K, 1.04; B, 0.29; C, 8.65; H, 1.05; N, 1.68 (%). Found: W, 58.65; Eu, 4.31; K, 1.34; B, 0.44; C, 8.46; H, 1.21; N, 1.45 (%). **5**. FTIR data (cm^{-1}): 3422(m), 3155(w), 3099(w), 2922 (w), 1637(m), 1591(m), 1408(m), 1247(w), 1001(w), 955(s), 904(s), 820(vs), 762(s), 687(m) and 530(m). Elemental analyses: Calcd for **6**: W, 58.90; Sm, 4.01; K, 1.04; B, 0.29; C, 8.65; H, 1.05; N, 1.68 (%). Found: W, 58.71; Sm, 3.96; K, 1.25; B, 0.39; C, 8.78; H, 1.24; N, 1.49 (%). **6**. FTIR data (cm^{-1}): 3443(m), 3098(w), 2921 (w), 1622(m), 1592(m), 1406(m), 1244(w), 1002(w), 956(s), 904(s), 821(vs), 762(s), 687(m) and 530(m).

X-ray Crystallography. Suitable single crystals with dimensions of 0.52 × 0.37 × 0.20 mm for **1**, 0.47 × 0.26 × 0.16 mm for **2**, 0.51 × 0.34 × 0.18 mm for **3**, 0.45 × 0.28 × 0.13 mm for **4**, 0.35 × 0.17 × 0.08 mm for **5** and 0.19 × 0.15 × 0.08 mm for **6**, were selected for single-crystal X-ray diffraction analysis. Empirical absorption correction was applied.

The structures of **1**−**6** were solved by the direct method and refined by the Full-matrix least-squares on F^2 using the SHELXTL-97 software.[23] All of the non-hydrogen atoms were refined anisotropically in **1** and **2**. The K cations and partial solvent water molecules OW11, OW12, OW13, OW15, OW16, OW17, and OW18 in **3**, and OW11 and OW12 in **4** exhibit unusual thermal parameters (U_{eq}) with the anisotropic refinement; thus, they were only isotropically refined. All of the non-hydrogen atoms were refined anisotropically in **5**. All of the non-hydrogen atoms, except disordered C26a and C26, were refined anisotropically in **6**. The hydrogen atoms attached to water molecules were not located in **1**−**6**. Positions of the hydrogen atoms attached to carbon atoms and those attached to nitrogen atoms, except C27 and C30 in **6**, were fixed in ideal positions in **3**−**6**. Site occupancies of the partial water molecules in **1**−**6** were set to be 1/2 through the refinement of their thermal parameters because of disorder. Compounds **1** and **2** contain an obvious site-occupancy disorder on the Ln3/K1 center with occupancy ratios of 50% for Ln3 and 50% for K1. The K1 atom in compound **3** is disordered into two positions, and each position has a site occupancy factor of 0.5. The borate centers of the POMs in **5** and **6** are all disordered. Other restraints such as ISOR and DELU were used in the refinements for obtaining reasonable atom sites and thermal parameters. A summary of the crystallographic data and structural determination for **1**−**5** is provided in Table 1. A summary of the crystallographic data and structural determination for **6** is provided in Supporting Information, Table S1. Selected bond lengths and angles of **1**−**5** are respectively listed in Supporting Information, Tables S2−S4.

CSD reference number: 421922 for **1** and 421921 for **2**. CCDC reference number: 782603 for **3** and 782606 for **4**, 782605 for **5** and 782607 for **6**.

Results and Discussion

Synthesis. The reactivity of the $[BW_{11}O_{39}H]^{8-}$ monovacant polyoxometalate and two different trivalent lanthanide cations (Ln = Ce^{3+}, Nd^{3+}) without or with organic ligands, has been investigated. Four compounds with two kinds of structures were obtained. Compounds **1** and **2** with 3D inorganic framework are made up of new polyoxoanions $[\{(H_2O)_4Ln(BW_{11}O_{39}H)\}_2]^{10-}$ and Ln^{3+} linkers. The only reported 1D inorganic chain, $H_2(NH_4)_{10}[Ce_2(BW_{11}O_{39})_2(H_2O)_6]\cdot 21H_2O$[21] based on 1:1 type substituted polyoxometaloborate cluster $[Ce(BW_{11}O_{39})(H_2O)_3]^{6-}$, similar to the compound $(NH_4)_5[Ce(SiW_{11}O_{39})(H_2O)_3]\cdot 8H_2O$ reported by Pope et al.,[12] was synthesized by the simple starting materials (sodium tungstate and boric acid). The

(23) (a) Sheldrick, G. M. *SHELXL 97, Program for Crystal Structure Refinement*; University of Göttingen: Göttingen, Germany, 1997; (b) Sheldrick, G. M. *SHELXL 97, Program for Crystal Structure Solution*; University of Göttingen: Göttingen, Germany, 1997.

Table 1. Crystal Data and Structure Refinements for **1**−**5**

	1	2	3	4	5
formula	$H_{106}B_2Ce_5KO_{130}W_{22}$	$H_{106}B_2Nd_5KO_{130}W_{22}$	$C_{12}H_{102}N_2B_2Ce_4K_2O_{126}W_{22}$	$C_{12}H_{104}N_2B_2Nd_4K_2O_{127}W_{22}$	$C_{54}H_{79}N_9B_2Eu_2K_2O_{114}W_{24}$
formula weight	6992.65	7013.25	6995.74	7030.23	7494.40
T (K)	293(2)	293(2)	293(2)	293(2)	293(2)
crystal system	monoclinic	monoclinic	monoclinic	monoclinic	triclinic
space group	$P2(1)/c$	$P2(1)/c$	$P2(1)/c$	$P2(1)/c$	$P\bar{1}$
a (Å)	17.8248(9)	17.857(4)	18.675(4)	18.6153(4)	12.014(2)
b (Å)	17.5528(1)	17.621(4)	17.471(4)	17.3568(4)	17.881(3)
c (Å)	22.0661(1)	22.093(4)	22.460(3)	22.3946(4)	18.689(3)
α (deg)	90	90	90	90	96.468(3)
β (deg)	120.052(3)	120.118(1)	121.781(1)	121.846(1)	107.600(2)
γ (deg)	90	90	90	90	103.057(3)
U (Å^3)	5975.8(5)	6013(2)	6229(2)	6146.5(2)	3656.5(1)
Z	2	2	2	2	1
μ (mm^{-1})	23.095	23.217	21.834	22.337	19.797
reflections collected	39561	27619	30700	40271	13908
independent reflections	10434	10540	10932	10815	8815
R(int)	0.0958	0.0742	0.0941	0.0621	0.0622
GOF on F^2	1.052	1.016	1.018	1.019	1.079
R_1[a] $[I > 2\sigma(I)]$	0.0712	0.0516	0.0531	0.0492	0.0699
wR_2[b] $[I > 2\sigma(I)]$	0.1594	0.1203	0.1187	0.1291	0.1650
R_1 (all data)	0.0858	0.0839	0.0784	0.0567	0.1152
wR_2 (all data)	0.1718	0.1389	0.1337	0.1357	0.1950

[a] $R1 = \sum||F_o| - |F_c||/\sum|F_o|$. [b] $wR2 = \sum[w(F_o^2 - F_c^2)^2]/\sum[w(F_o^2)^2]^{1/2}$.

presynthesized monovacant polyoxoanion was in favor of the assembly of high-dimensional structure. When pyridine-4-carboxylic acid molecule was used to substitute the coordinated water molecules of lanthanide ions, compounds **3** and **4** with 3D framework made up of new polyoxoanions $[\{(H_2O)_4Ln(BW_{11}O_{39}H)\}_2]^{10-}$ and Ln-pyridine-4-carboxylic acid linkers were obtained. Although this method has been put forward to prepare new hybrids by Mialane et al.,[3] few successful examples, especially 3D structures, have been reported up to now. Many parallel experiments prove that the quality of crystals depends on the pH value and stoichiometry. The pH of the reaction is a determining factor and the optimal pH is 3.5. For a low pH (pH < 2.5) no reaction occurs, a higher pH increases the yield and the kinetics of the reaction. The pH should, however, not exceed 4.0 as the hydrolysis of the lanthanide cation easily occurs at higher pH values. The products are obviously affected by the stoichiometry of $Ln^{3+}/[BW_{11}O_{39}H]^{8-}$. Compounds **1**−**4** can be isolated by the 4:1 $Ln^{3+}/[BW_{11}O_{39}H]^{8-}$ ratio, and the excess Ln-(NO_3) ensures high yields of the desired products. When the $Ln^{3+}/[BW_{11}O_{39}H]^{8-}$ ratio decreased from 4:1 to 3:1 or 2:1, only yields of compounds **1**−**4** were reduced, and no discrete 1:2 LSPs can be obtained, differing from those reactions between $[SiW_{11}O_{39}]^{8-}$ or $[PW_{11}O_{39}]^{7-}$ and lanthanide cations reported by Pope and Niu et al.

Interestingly, when Eu^{3+} and Sm^{3+} cations were utilized instead of Ce^{3+} or Nd^{3+} ions in **3** and **4** under the similar condition, a structure different from the above is obtained, $(C_6NO_2H_5)H_2K_2[(C_6NO_2H_5)_4Ln(H_2O)_2]_2[BW_{12}O_{40}]_2 \cdot 12H_2O$ (Ln = Eu **5**, Sm **6**). Compounds **5** and **6** are isostructural, possessing a 3D supramolecular channel framework constructed from the α_1-type Keggin anions $[BW_{12}O_{40}]^{5-}$ and dinuclear lanthanide-organic coordination complex fragments. Remarkably, the structural variation from the 3D open frameworks in **3** and **4** into the 3D supramolecular channel networks in **5** and **6** is attributed to the lanthanide contraction effect. Luminescence measurement of **5** exhibits red fluorescent emission of the Eu^{3+} ion at room temperature.

Crystal Structures of 1 and 2. The single crystal X-ray diffraction analyses reveal that compounds **1** and **2** are isostructural, and the unit cell dimensions, volumes, related bond distances and angles are only slightly changed. The structure of the two composite compounds exhibits an unusual 3D open framework composed of $[\{(H_2O)_4Ln(BW_{11}O_{39}H)\}_2]^{10-}$ polyoxoanions, Ln^{3+} cations (Ln = Ce **1** and Nd **2**), K^+ cations and lattice water molecules. The $[\{(H_2O)_4Ln(BW_{11}O_{39}H)\}_2]^{10-}$ cluster is a lanthanide-substituted double-Keggin-type polyoxoanion. Each polyoxoanion contains two $[\alpha\text{-}BW_{11}O_{39}H]^{8-}$ subunits connected by two Ln centers via Ln−O−W bonds, and an inversion center relating the $[(H_2O)_4Ln(BW_{11}O_{39}H)]^{5-}$ parts. Monovacant Keggin-type $[\alpha\text{-}BW_{11}O_{39}H]^{8-}$ anions can be viewed as removal of a W−Ot group from the $[\alpha\text{-}BW_{12}O_{40}]^{5-}$ anion, which consists of a central $\{BO_4\}$ tetrahedron surrounded by four vertex-sharing M_3O_{13} trimers (see Figure 1a). Four kinds of oxygen atoms exist in the cluster according to the manner of oxygen coordination, that is central oxygen Oa, double-bridging oxygen Ob,c, terminal oxygen Ot, terminal oxygen linked to Ln^{3+} Ot′. Thus the W−O distances can be grouped into four sets: W−Oa 2.287(1)−2.461(1) Å, W−Ob,c 1.827(1)−2.110(1) Å, W−Ot 1.701(1)−1.726(1) Å, W−Ot′ 1.722(1)−1.767(1) Å in **1**; W−Oa 2.291(1)−2.457(1) Å, W−Ob,c 1.826(1)−2.087(1) Å, W−Ot 1.709(1)−1.735(1) Å, W−Ot′ 1.714(1)−1.790(1) Å in **2**. The central B−Oa distances vary from 1.49(2) to 1.56(2) Å in **1** and from 1.48(2) to 1.57(2) Å in **2**, which corresponds with that of $H_2(NH_4)_{10}[Ce_2(BW_{11}O_{39})_2(H_2O)_6] \cdot 21H_2O$. The bond angles of O−B−O range from 105.5(1) to 113.9(1) ° in **1**, and from 105.8(1) to 114.5(1) ° in **2** respectively. The B atoms reside in the center of $\{BO_4\}$ tetrahedra, which are somewhat distorted resulting from the removal of one W−Ot group and the incorporation of one Ln cation into the monovacant

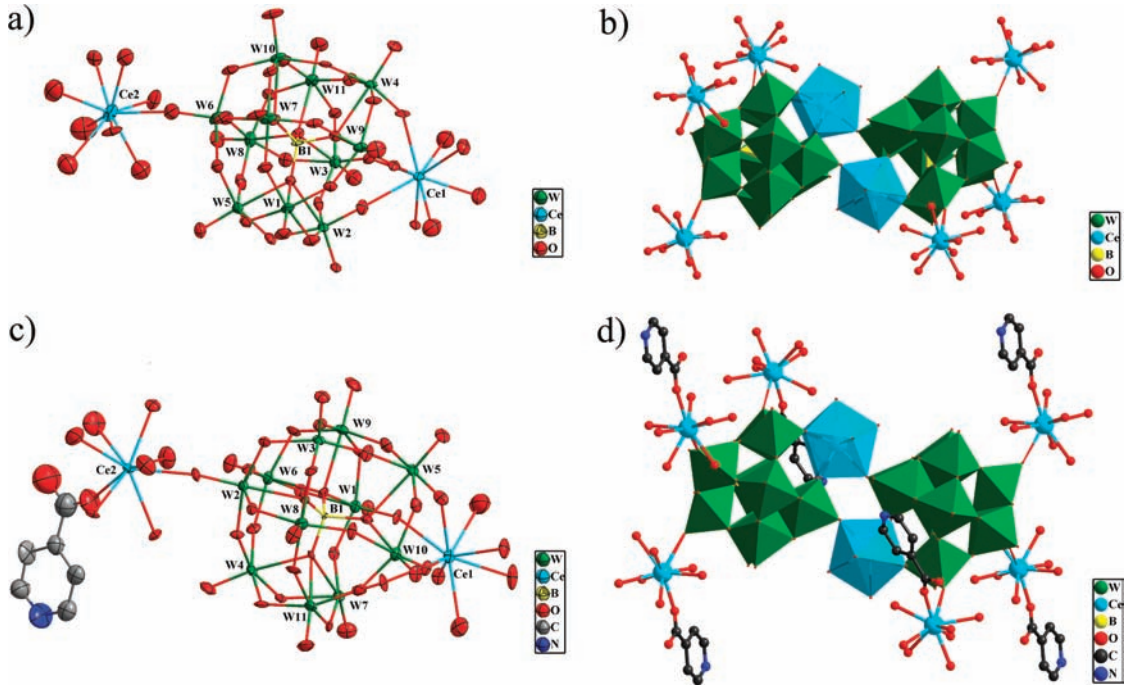

Figure 1. (a) ORTEP drawing of compound **1** with thermal ellipsoids at 50% probability. Other molecules are omitted for clarity. (b) Polyhedron and ball-stick view of the lanthanide-substituted double-Keggin-type polyoxoanions $[\{(H_2O)_4Ln(BW_{11}O_{39}H)\}_2]^{10-}$ and its coordination environment in **1**. (c) ORTEP drawing of compound **3** with thermal ellipsoids at 50% probability. Other molecules are omitted for clarity. (d) View of the lanthanide-substituted double-Keggin-type polyoxoanions $[\{(H_2O)_4Ln(BW_{11}O_{39}H)\}_2]^{10-}$ and its coordination environment in **3**.

POM framework as compared to the saturated Keggin structure.[24]

There are three crystallographically unique Ln(III) (Ln = Ce **1** and Nd **2**) cations in the complex unit. The Ln(1) cation, incorporated to the vacant site of the $[\alpha\text{-}BW_{11}O_{39}H]^{8-}$ unit in the "cap" region to form the $[\{(H_2O)_4Ln(BW_{11}O_{39}H)\}_2]^{10-}$ cluster, is nine-coordinate, adopting a distorted monocapped square antiprismatic coordination environment (the coordination environment of Ce^{3+} in **1** shown in Figure 1a-b) bonding to four oxygen atoms from the defect site of one $[\alpha\text{-}BW_{11}O_{39}H]^{8-}$ anion [Ce−O 2.483(1)−2.537(1), Nd−O 2.448(1)−2.502(1) Å], four water molecules [Ce−OW 2.496(1)−2.571(1), Nd-OW 2.476(1)−2.567(1) Å], and one terminal oxygen atom from the other $[(H_2O)_4Ln(BW_{11}O_{39}H)]^{5-}$ moiety [Ce−O 2.499(1), Nd−O 2.502(1) Å]. The lanthanide-substituted double-Keggin-type polyoxoanion $[\{(H_2O)_4Ln(BW_{11}O_{39}H)\}_2]^{10-}$ in **1** and **2** is somewhat similar with the dimeric cores of $[\{(\alpha\text{-}PW_{11}O_{39}H)Nd(H_2O)_3\}_2]^{6-}$ and $[SiW_{11}CeO_{39}]^{4-}$ reported by Niu et al. and Hill et al., respectively;[10a,25] however, the Nd cations incorporated to the vacant site of $[\alpha\text{-}PW_{11}O_{39}H]^{6-}$ unit and Ce cations incorporated to the $[SiW_{11}O_{39}]^{8-}$ are eight-coordinate, different from the nine-coordinate Ln(1) cation in **1** and **2**. The polyoxoanion $[\{(H_2O)_4Ln(BW_{11}O_{39}H)\}_2]^{10-}$ represents the first 2:2-type monovacant Keggin polyoxotungstate dimers constituted by two $[\alpha\text{-}BW_{11}O_{39}H]^{8-}$ polyoxoanions and two lanthanide cations. Ln(2) cation, joined neighboring $[\{(H_2O)_4Ln(BW_{11}O_{39}H)\}_2]^{10-}$ polyoxoanions together as linker, has a tricapped trigonal prism coordination environment, defined by three terminal oxygen atoms from three $[\{(H_2O)_4Ln(BW_{11}O_{39}H)\}_2]^{10-}$ units [Ce−O 2.495(1)−2.501(1), Nd−O 2.460(1)−2.500(2) Å], and six water molecules [Ce−OW 2.513(2)−2.610(2), Nd−O 2.478(2)−2.590(2) Å]. Ln(3) cation, weakly bonded to $[\{(H_2O)_4Ln(BW_{11}O_{39}H)\}_2]^{10-}$ polyoxoanions [Ce−O 2.728(1)−2.766(1), Nd−O 2.720(1) Å], is site occupancy disordered, and the position is occupied by Ln and K atom with an occupancy factor 0.5. This kind of disorder has been found in the crystal structure $K_{0.5}Nd_{0.5}[Nd_2(SiW_{11}O_{39})(H_2O)_{11}]$ with polyoxoanions surrounded by Nd^{3+}/K^+ cations described by Mialane, Sécheresse, and coworkers.[13] The average Ce−O bond length is 2.526 Å in **1** and Nd−O 2.508 Å in **2** (considering the coordinated Ln(1) and Ln(2)). The average Ce−O bond length in **1** is larger than Nd−O in **2**.

Intriguingly, in **1** and **2**, lanthanide-substituted double-Keggin-type polyoxoanions $[\{(H_2O)_4Ln(BW_{11}O_{39}H)\}_2]^{10-}$ as building blocks are first linked by Ln^{3+} (Ln = Ce **1** and Nd **2**) cations to generate a 1D wavelike chain (Figure 2a). There are two kinds of such 1D chain according to the different orientations of double-Keggin-type polyoxoanions in the chain. These two kinds of chains are further interconnected by other Ln^{3+} cations to generate a 2D layer in an ABAB$\cdots$ mode along the *c* axis (shown in Figure 2b). Furthermore, these 2D sheets are further joined together via the Ln−O−W bonds to form a 3D open framework (shown in Figure 3). It is notable that this kind of connection modes results in the formation of 1D channels, which were occupied by free water molecules. The dimensions of the channels are about 12.1 × 7.4 Å in **1** and 12.1 × 7.3 Å in **2** along the *c* axis (Supporting Information, Figure S2). Free water molecules are filled in the channels and participate in the extensive

(24) An, H. Y.; Wang, E. B.; Xiao, D. R.; Li, Y. G.; Su, Z. M.; Xu, L. *Angew. Chem., Int. Ed.* **2006**, *45*, 904.
(25) Kholdeeva, O. A.; Timofeeva, M. N.; Maksimov, G. M.; Maksimovskaya, R. I.; Neiwert, W. A.; Hill, C. L. *Inorg. Chem.* **2005**, *44*, 666.

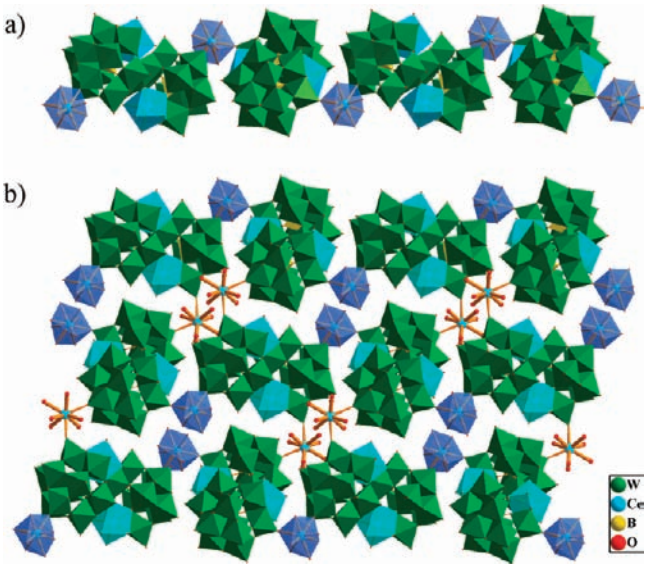

Figure 2. (a) Polyhedron view of the 1D linear chain in **1**. (b) 2D sheet of **1**, showing the 1D chains linked by other Ce^{3+} cations (color code: B, yellow; W, green; Ce, blue; O, red).

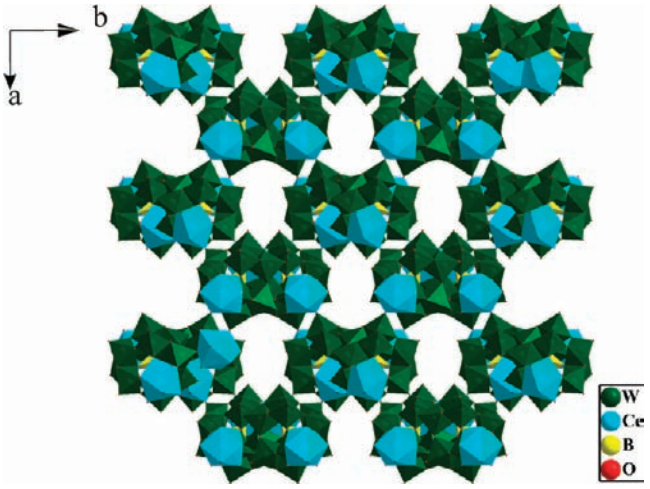

Figure 3. View along the *c* axis illustrating the 3D open framework with channels in **1** (color code: B, yellow; W, green; Ce, blue; O, red). Free water molecules situated in the channels are omitted for clarity.

hydrogen-bonding interactions with the polyoxoanion framework. To our best knowledge, compounds **1** and **2** represent the first examples of 3D inorganic architectures based on lanthanide-substituted POMs. From the view of topology, the $[\{(H_2O)_4Ln(BW_{11}O_{39}H)\}_2]^{10-}$ unit is covalently bonded to six adjacent Ln(2) cations, and each Ln(2) cation is linked with three $[\{(H_2O)_4Ln(BW_{11}O_{39}H)\}_2]^{10-}$ units. Therefore, the overall 3D framework can be rationalized as a (3,6)-connected net by assigning the Ln(2) subunits and $[\{(H_2O)_4Ln(BW_{11}O_{39}H)\}_2]^{10-}$ as three-connected nodes and six-connected nodes (Figure 4). The Schläfli symbol of this network is $(4\cdot6^2)_2(4^2\cdot6^{10}\cdot8^3)$, the same as the rutile.[26]

When pyridine-4-carboxylic acid was introduced to substitute the coordinated water molecules in **1** and **2**, 3D hybrid compounds **3** and **4** were obtained.

(26) Qin, C.; Wang, X. L.; Wang, E. B.; Su, Z. M. *Inorg. Chem.* **2005**, *44*, 7122.

Crystal Structures of 3 and 4. The single crystal X-ray diffraction analyses reveal that compounds **3** and **4** are isostructural, and the unit cell dimensions, volumes, related bond distances and angles are only slightly changed. The structure of the two composite compounds exhibits a 3D open framework composed of $[\{(H_2O)_4Ln(BW_{11}O_{39}H)\}_2]^{10-}$ polyoxoanions, Ln−pyridine-4-carboxylic acid coordination complexes (Ln = Ce **3** and Nd **4**), K^+ cations and lattice water molecules. The $[\{(H_2O)_4Ln(BW_{11}O_{39}H)\}_2]^{10-}$ cluster is also a lanthanide-substituted double-Keggin-type polyoxoanion, similar to compounds **1** and **2**. Four kinds of oxygen atoms exist in the cluster according to the manner of oxygen coordination, that is central oxygen Oa, double-bridging oxygen Ob,c, terminal oxygen Ot, terminal oxygen linked to Ln^{3+} Ot′. Thus the W−O distances can be grouped into four sets: W−Oa 2.245(1)−2.445(1) Å, W−Ob,c 1.812(1)−2.100(1) Å, W−Ot 1.704(1)−1.728(1) Å, W−Ot′ 1.728(1)−1.776(1) Å in **3**; W−Oa 2.258(9)−2.471(9) Å, W−Ob,c 1.818(9)−2.097(9) Å, W−Ot 1.693(1)−1.738(1) Å, W−Ot′ 1.723(9)−1.767(9) Å in **4**. The central B−Oa distances vary from 1.49(2) to 1.57(2) Å in **3** and from 1.478(2) to 1.555(2) Å in **4**. The bond angles of O−B−O range from 106.6(1) to 113.6(1)° in **3**, and from 106.1(1) to 112.8(1)° in **4** respectively, indicating that the $\{BO_4\}$ tetrahedra are distorted to a similar extent in each case.

There are two crystallographically unique Ln(III) (Ln = Ce **3** and Nd **4**) cations in the complex unit. Ln(1) incorporated to the vacant site of the $[\alpha\text{-}BW_{11}O_{39}H]^{8-}$ unit, links to four oxygen atoms from one $[\alpha\text{-}BW_{11}O_{39}H]^{8-}$ anion [Ce−O 2.457(1)−2.534(1), Nd−O 2.427(9)−2.512(9) Å], four water molecules [Ce−OW 2.496(2)−2.594(2), Nd−OW 2.468(1)−2.531(1) Å], and one terminal oxygen atom from the other $[(H_2O)_4Ln(BW_{11}O_{39}H)]^{5-}$ moiety [Ce−O 2.480(1), Nd−O 2.462(1) Å], adopting a distorted monocapped square antiprismatic coordination environment (the coordination environment of Ce^{3+} in **3** shown in Figure 1c-d). Ln(2) has a tricapped trigonal prism coordination environment, defined by three terminal oxygen atoms from three $[\{(H_2O)_4Ln(BW_{11}O_{39}H)\}_2]^{10-}$ units [Ce−O 2.449(1)−2.475(1), Nd−O 2.416(1)−2.468(1) Å], one carboxyl oxygen atom from one pyridine-4-carboxylic acid molecules [Ce−O 2.389(2), Nd−O 2.387(1) Å] and five water molecules [Ce−OW 2.536(1)−2.630(2), Nd−OW 2.516(9)−2.598(1) Å]. The average Ce−O bond length is 2.527 Å in **3** and Nd−O is 2.493 Å in **4**. The average Ce−O bond length is larger than Nd−O. There is one crystallographically independent pyridine-4-carboxylic acid molecule, which adopts a monodentate coordination fashion and coordinates to one Ln(III) cation by utilizing its carboxyl oxygen atom.

In **3** and **4**, lanthanide-substituted double-Keggin-type polyoxoanions $[\{(H_2O)_4Ln(BW_{11}O_{39}H)\}_2]^{10-}$ are first linked by Ln-pyridine-4-carboxylic acid complexes (Ln = Ce **3** and Nd **4**) to generate a 1D wavelike chain (Figure 5a). Adjacent chains are further interconnected by other Ln-pyridine-4-carboxylic acid fragments to generate a 2D layer (shown in Figure 5b). Furthermore, neighboring 2D sheets are further joined together via the Ln−O−W bonds to form a 3D open framework (Figure 6). Notably, this kind of connection modes results in the formation of 1D channels, which were also occupied by free water molecules. The dimensions of the channels are about

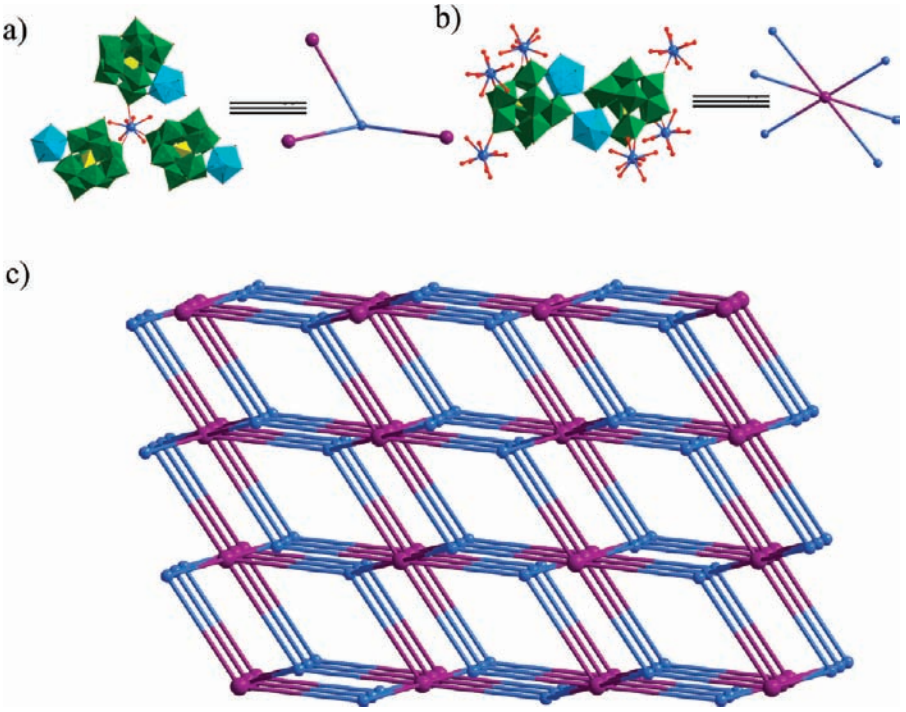

Figure 4. (a) 3-connected Ce^{3+} node linked with three $[\{(H_2O)_4Ln(BW_{11}O_{39}H)\}_2]^{10-}$ clusters. (b) 6-connected $[\{(H_2O)_4Ln(BW_{11}O_{39}H)\}_2]^{10-}$ unit coordinated with six Ce^{3+} cations. (c) Schematic representation of the rutile topology of compound **1**.

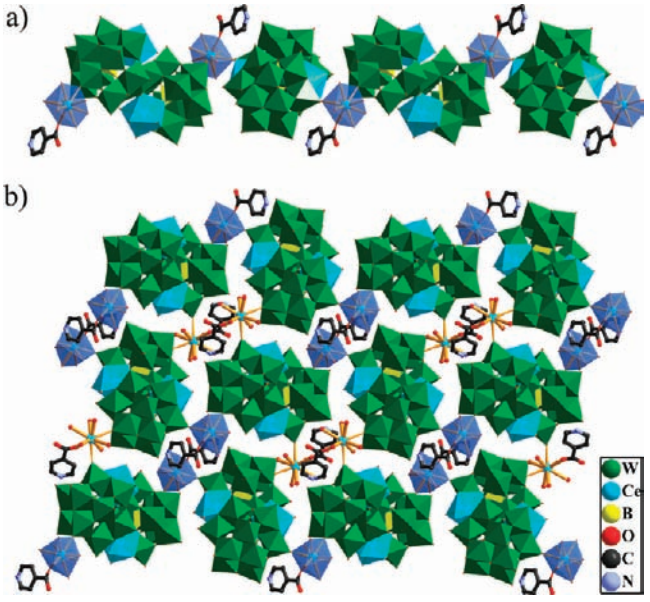

Figure 5. (a) Polyhedron view of the 1D linear chain in **3**. (b) 2D sheet of **3**, showing the 1D chains linked by other Ce-pyridine-4-carboxylic acid molecules (color code: B, yellow; W, green; Ce, blue; O, red; N, oxford blue; C, dark gray).

12.2×7.6 Å in **3** and 12.2×7.5 in **4** along the *c* axis (shown in Supporting Information, Figure S3). Free water molecules are filled in the channels and participate in the extensive hydrogen-bonding interactions with the polyoxoanions and ligands. To our knowledge, compounds **3** and **4** represent the first examples of 3D hybrid architectures based on lanthanide-substituted POMs. Remarkably, in **3** and **4** the $[\{(H_2O)_4Ln(BW_{11}O_{39}H)\}_2]^{10-}$ polyoxoanions were linked up by $[Ln(C_6NO_2H_5)]^{3+}$ fragments to form a 3D framework, whereas in **1** and **2** the

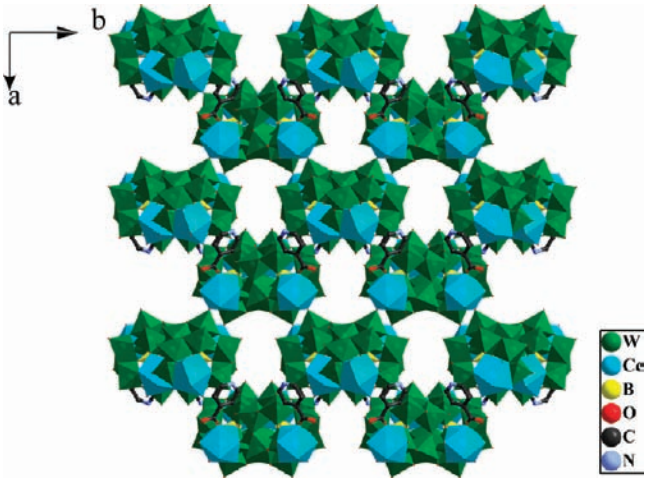

Figure 6. View along the *c* axis illustrating the 3D open framework with 1D channels in **3** (color code: B, yellow; W, green; Ce, blue; O, red; N, oxford blue; C, dark gray). Free water molecules situated in the channels are omitted for clarity.

$[\{(H_2O)_4Ln(BW_{11}O_{39}H)\}_2]^{10-}$ polyoxoanions were linked up by $[Ln(H_2O)_6]^{3+}$ units to form a 3D structure. The greatest structural difference between compounds **1**, **2** and **3**, **4** is caused by the pyridine-4-carboxylic acid molecule substituting one coordinated water molecule. Furthermore, the pyridine-4-carboxylic acid molecule can only substitute one water molecule coordinated to the bridging lanthanide cation, and can not substitute the water molecules coordinated to the lanthanide cation incorporated to the vacant site of the $[\alpha\text{-}BW_{11}O_{39}H]^{8-}$ unit, owing to the steric encumbrance. From the view of topology, the overall 3D framework of compounds **3** and **4** can also be rationalized as a (3,6)-connected rutile net with Schläfli symbol $(4\cdot6^2)_2(4^2\cdot6^{10}\cdot8^3)$ by assigning the Ln-pyridine-4-carboxylic acid subunits

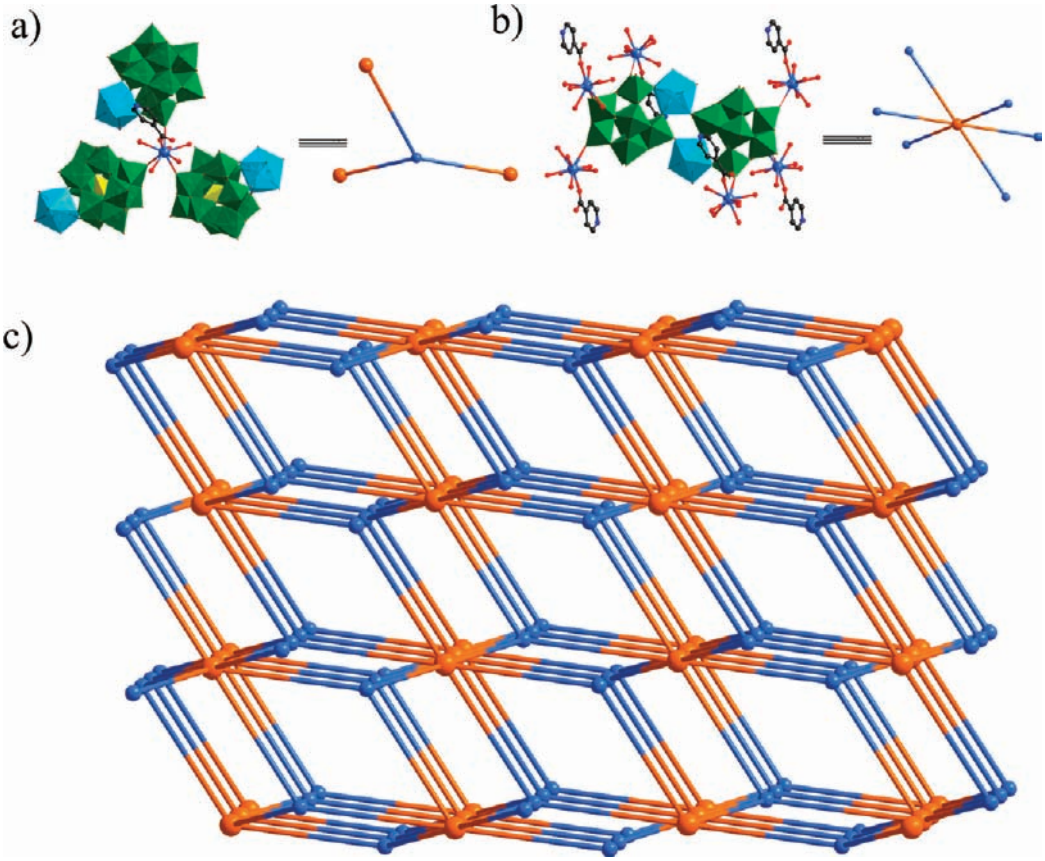

Figure 7. (a) 3-connected Ce-pyridine-4-carboxylic acid node linked with three $[\{(H_2O)_4Ln(BW_{11}O_{39}H)\}_2]^{10-}$ clusters. (b) 6-connected $[\{(H_2O)_4Ln(BW_{11}O_{39}H)\}_2]^{10-}$ cluster coordinated with six Ce-pyridine-4-carboxylic acid units. (c) Schematic representation of the rutile topology of the compound **3**.

and $[\{(H_2O)_4Ln(BW_{11}O_{39}H)\}_2]^{10-}$ clusters as three-connected nodes and six-connected nodes (Figure 7).

When Eu^{3+} and Sm^{3+} cations were utitilized in place of Ce^{3+} and Nd^{3+} cations under the similar reaction condition with compounds **3** and **4**, two isostructural compounds **5** and **6** were obtained, which possess entirely different structures from **3** and **4**.

Crystal Structures of Compounds 5 and 6. X-ray crystallography shows that compounds **5** and **6** are isostructural, and the unit cell dimensions and volumes are slightly changed. Herein only the structure of compound **5** will be discussed in detail, owing to the poor crystal data of compound **6**. The structure of compound **5** is a 3D supramolecular open framework constructed from $[BW_{12}O_{40}]^{5-}$ building blocks and dimeric Eu-pyridine-4-carboxylic acid cations, with pyridine-4-carboxylic acid molecules and lattice water molecules residing in the channels. The $[BW_{12}O_{40}]^{5-}$ cluster is a classic Keggin structure, which consists of a central $\{BO_4\}$ tetrahedron surrounded by four vertex-sharing M_3O_{13} trimers (see Supporting Information, Figure S4). Each M_3O_{13} group is composed of three $\{WO_6\}$ octahedra linked in a triangular arrangement by sharing edges. Three kinds of oxygen atoms exist in the cluster according to the way the oxygen atoms are coordinated: central oxygen Oa, double-bridging oxygen Ob,c, terminal oxygen Ot. Thus, the W−O bond lengths fall into three classes: W−Oa 2.34(3)−2.51(3), W−Ob,c 1.82(2)−1.97(3), and W−Ot 1.61(2)−1.73(3) Å in **5**. The central B−Oa distances vary from 1.40(4) to 1.63(3) Å in **5**. The bond angles of O−B−O range from 62.1(2)−180.0(4)° in **5**. Notably, for the $\{BO_4\}$ group in **5**, each of four oxygen atoms is disordered over two positions. Similar disordered phenomena have been reported in the previous studies.[27]

The asymmetric unit in the structure of **5** consists of two crystallographically independent one-half Keggin anions, in which both B ions (B(1) and B(2)) occupy special positions (Supporting Information, Figure S4), and one crystallographically independent mononuclear $[Eu(C_6NO_2H_5)_4]^{3+}$ fragment. Two mononuclear $[Eu(C_6NO_2H_5)_4]^{3+}$ clusters are joined together into a molecular dimer $[Eu_2(C_6NO_2H_5)_8]^{6+}$ related by a crystallographic inversion center. One crystallographically unique Eu(III), residing in a distorted square antiprismatic coordination environment, is defined by six carboxyl oxygen atoms from six pyridine-4-carboxylic acid units and two water molecules [Eu(1)−O 2.30(2)−2.46(2), Eu(1)−OW 2.456(2)−2.56(2) Å]. The average Eu−O bond length is 2.397 Å, in the range of covalent bonds according to the literatures.[26] There are four crystallographically independent coordinating pyridine-4-carboxylic acid molecules, which adopt two kinds of coordination modes including monodentate and bidentate coordination fashion, and bridge two neighboring Eu(III) cations by utilizing its carboxyl oxygen atoms.

In **5**, these dimers are joined up together by hydrogen-bonding interactions (O52···N1 2.684 Å) to form a 1D supramolecular chains, then the $[BW_{12}O_{40}]^{5-}$ anions are

(27) Xu, Y.; Nie, L.; Zhang, G.; Chen, Q.; Zheng, X. *Inorg. Chem. Commun.* **2006**, *9*, 329.

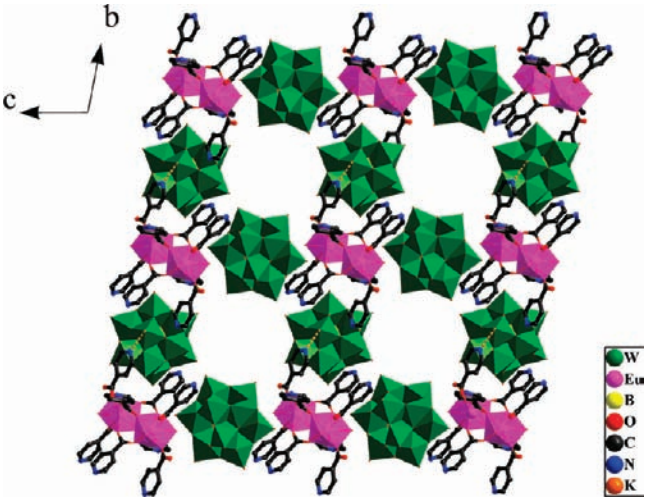

Figure 8. Polyhedral and ball-stick view along the *a* axis illustrating the 3D supramolecular channel structure of **5** (color code: B, yellow; W, green; Eu, purple; O, red; N, oxford blue; C, dark gray).

linked together by $[Eu_2(C_6NO_2H_5)_8]^{6+}$ chains to form an interesting 2D supramolecular network on the *ac* plane (see Supporting Information, Figure S5). Furthermore, adjacent layers are pillared by other Keggin polyoxoanions to yield a 3D supramolecular channel structure via hydrogen-bonding interactions (O18···N4 2.871 Å). The dimensions of the channels are about 13.3×9.5 Å in **5** along the *a* axis (shown in Figure 8). Pyridine-4-carboxylic acid molecules, K^+ cations and isolated water molecules are situated in the channels, and participate in the extensive hydrogen-bonding interactions with the host framework.

Structural Comparison of the Frameworks 3−6. Compounds **3**, **4** and **5**, **6** were obtained by conventional synthesis method under the similar reaction condition. The obvious structural difference between compounds **3**, **4** and **5**, **6** is due to the introduction of different lanthanides that have different ionic radius and coordination geometry to result in the formation of different hybrid structures. In compounds **3** and **4**, Ce^{3+} and Nd^{3+} cations with the bigger ionic radius compared to the Eu^{3+} and Sm^{3+}, are nine-coordinate and coordinate to the vacant site of $[BW_{11}O_{39}H]^{8-}$ forming a $[\{(H_2O)_4Ln(BW_{11}O_{39}H)\}_2]^{10-}$, whereas in compounds **5** and **6**, Eu^{3+} and Sm^{3+} cations which can not coordinate to the vacant site of $[BW_{11}O_{39}H]^{8-}$, are eight-coordinate and link to pyridine-4-carboxylic acid ligands. Interestingly, in the synthesis procedure of the compounds **5** and **6**, we found that the precursor $[BW_{11}O_{39}H]^{8-}$ was transformed to the saturated polyoxoanion $[BW_{12}O_{40}]^{5-}$. Only one crystal structure has been characterized to prove the phenomenon by Cadot's group to date.[28] This phenomenon has also been found in our research on the reactivity of $[BW_{11}O_{39}H]^{8-}$ and transition metal cations. The successful synthesis of compounds **3**−**6** has further demonstrated that the lanthanide contraction effect plays a critical directing role in the frameworks' dimensional degressive variation from the 3D frameworks into the 0D networks.[13]

The bond valence sum calculations indicate that B site is in the +3 oxidation state, Ce, Nd, Eu and Sm sites are in the +3 oxidation state, and all W sites are in the +6 oxidation state.[29]

FT-IR Spectra. In the IR spectrum of compound **1**, the features at 946, 851, and 790 cm^{-1} are attributed to ν(W−Ot), ν(W−Ob) and ν(W−Oc) of the $[\alpha\text{-}BW_{11}O_{39}H]^{8-}$ polyoxoanion[21,30] (see Supporting Information, Figure S6a). The IR spectrum of compound **2** is similar to that of **1** (see Supporting Information, Figure S6b). In the IR spectrum of compound **3**, the features at 1600 and 1397 cm^{-1} can be regarded as the asymmetric and symmetric stretching vibrations of the carboxylate group of pyridine-4-carboxylic acid molecule.[31] The absence of strong peaks around 1720 cm^{-1} indicates that all carboxylic groups are deprotonated. The difference between $\nu_{as}(CO^{2-})$ and $\nu_s(CO^{2-})$ in the IR spectrum has been successfully used to derive information regarding bonding modes of carboxylate anions.[32] The $\Delta\nu$ of 203 cm^{-1} indicated the monodentate coordination mode of carboxylate group in **3**, which is consistent with the results of the X-ray analysis. The peaks at 946, 851, and 792 cm^{-1} are attributed to ν(W−Ot), ν(W−Ob) and ν(W−Oc) of the $[\alpha\text{-}BW_{11}O_{39}H]^{8-}$ polyoxoanion (see Supporting Information, Figure S6c). The IR spectrum of compound **4** is similar to that of **3** (see Supporting Information, Figure S6d). The wavenumber of the main bands of $[BW_{12}O_{40}]^{5-}$ of **5** and **6** shifts to some extent in $[BW_{11}O_{39}H]^{8-}$ of **3** and **4** compared with those in the literature.[33] In the IR spectrum of compound **5**, the features at 3422−1247 cm^{-1} can be regarded as characteristics of the pyridine-4-carboxylic acid molecule. The peaks at 955, 904, and 820 cm^{-1} are attributed to ν(W−Ot), ν(B−Oa), and ν(W−Oc) of the $[BW_{12}O_{40}]^{5-}$ polyoxoanion[24,30] (see Supporting Information, Figure S6e). The IR spectrum of compound **6** is similar to that of **5** (see Supporting Information, Figure S6f).

TG Analyses. The thermogravimetric (TG) curve of **1** is shown in the Supporting Information, Figure S7a. It exhibits a two-step continuous weight loss process and gives a total weight loss of 14.1% in the range of 43−800 °C, which agrees with the calculated value of 13.6%. The weight loss of 12.7% from 43 to 300 °C corresponds to the loss of all lattice and partial coordinated water molecules. The weight loss of 1.4% from 350 to 600 °C corresponds to the loss of residual coordinated water molecules. The TG curve of compound **2** exhibits similar weight loss stages to those of compound **1** (see Supporting Information, Figure S7b). In **2** the whole weight loss (14.2%) at 48−600 °C is in agreement with the calculated value (13.6%).

The TG curve of **3** is shown in the Supporting Information, Figure S7c. It exhibits a three-step continuous weight loss process and gives a total weight loss of 16.0% in the range of 44−800 °C, which agrees with the calculated

(28) Leclerc-Laronze, N.; Marrot, J.; Hervé, G.; Thouvenot, R.; Cadot, E. *Chem.—Eur. J.* **2007**, *13*, 7234.

(29) Brown, I. D.; Altermatt, D. *Acta. Crystallogr., Sect. B* **1985**, *41*, 244.

(30) (a) Rocchiccioli-Deltcheff, C.; Fournier, M.; Franck, R.; Thouvenot, R. *Inorg. Chem.* **1983**, *22*, 207. (b) Uchida, S.; Kawamoto, R.; Mizuno, N. *Inorg. Chem.* **2006**, *45*, 5136.

(31) Chen, W. T.; Fukuzumi, S. C. *Inorg. Chem.* **2009**, *48*, 3800.

(32) (a) Deacon, G. B.; Phillips, R. *Coord. Chem. Rev.* **1980**, *33*, 227. (b) Li, C. H.; Huang, K. L.; Chi, Y. N.; Liu, X.; Han, Z. G.; Shen, L.; Hu, C. W. *Inorg. Chem.* **2009**, *48*, 2010.

(33) Niu, Y. J.; Liu, B.; Xue, G. L.; Hu, H. M.; Fu, F.; Wang, J. W. *Inorg. Chem. Commun.* **2009**, *12*, 853.

value of 15.4%. The weight loss of 10.8% from 44 to 280 °C corresponds to the loss of all lattice and partial coordinated water molecules. The weight loss of 1.5% from 295 to 550 °C corresponds to the loss of residual coordinated water molecules. The whole weight loss of 12.3% at 44−550 °C corresponds to the loss of all lattice and coordinated water molecules (calcd 11.8%). The weight loss of 3.7% at 590−700 °C arises from the decomposition of organic molecules (calcd 3.5%). The TG curve of compound **4** exhibits similar weight loss stages to those of compound **3** (see Supporting Information, Figure S7d). In **4** the whole weight loss (15.8%) at 36−700 °C is in agreement with the calculated value (15.5%).

The TG curve of **5** is shown in the Supporting Information, Figure S7e. It gives a total weight loss of 19.5% in the range of 44−1000 °C, which agrees with the calculated value of 18.9%. The weight loss of 4.5% at 44−300 °C corresponds to the loss of all lattice and coordinated water molecules (calcd 4.1%). The weight loss of 15.0% at 310−980 °C arises from the decomposition of organic molecules (calcd 14.8%). The TG curve of compound **6** exhibits similar weight loss stages to those of compound **5**. In **6** the whole weight loss (19.2%) is in agreement with the calculated value (18.9%) (Supporting Information, Figure S7f).

PXRD Characterization. The PXRD patterns for compounds **1**−**6** are presented in the Supporting Information, Figure S8. The diffraction peaks of both calculated and experimental patterns match well, indicating the phase purities of these compounds. The PXRD patterns for **1** and **2** are very similar, emphasizing the isostructural nature of the two compounds. The PXRD patterns for **3** and **4** are also very similar, showing the isostructural nature of two compounds. The similarity of PXRD patterns of compounds **5** and **6** also indicate that the two compounds are isostructural. These conclusions are in agreement with the results of the single crystal X-ray analysis.

Magnetic Properties of Compounds 1−4. The magnetic susceptibilities of compounds **1**−**4** were measured in the 2−300 K temperature range under a 1 KOe applied field and are shown as $\chi_M T$ and $1/\chi_M$ versus T plots in Figures 9a−9d. It is noted that the $4f^n$ configuration of a Ln^{3+} ion, except for Gd^{3+}, is split into $^{2S+1}L_J$ states by the interelectronic repulsion and the spin−orbit coupling. Further splitting into Stark components is caused by the crystal-field perturbation. So the variable-temperature magnetic properties of a free Ln^{3+} ion generally strongly deviate from the Curie law, and $\chi_M T$ decreases with the system cooling because of the depopulation of the Stark levels.[34]

For **1**, the $\chi_M T$ value at 300 K is 3.15 emu K mol^{-1} (5.02 μ_B), which is slightly lower than the expected value 4.02 emu K mol^{-1} (5.67 μ_B, considering $g = 6/7$) of five isolated Ce^{3+} ions in the $^2F_{5/2}$ ground state. When decreasing the temperature, $\chi_M T$ products of **1** decrease gradually to the minimum of 1.81 emu K mol^{-1} at 2 K. The magnetic behavior of **1** does not follow the Curie law. In the temperature range of 2−300 K, the magnetic susceptibility of **1** obeys the Curie−Weiss law. Curve fits for $1/\chi_M$ versus T plots of **1** with the Curie−Weiss law in the range 2−300 K results in $C = 3.27$ emu K mol^{-1} and $\theta = -11.03$ K. The whole profile of the $\chi_M T$ versus T curve is not indicative of the nature of the interactions between Ce(III) ions because of the crystal-field effect, which splits the 6-fold degenerate $^2F_{5/2}$ ground state into Stark levels, and the values of $\chi_M T$ mainly depend on the populations of those Stark levels. At 300 K, all the Stark levels from the 6-fold degenerate $^2F_{5/2}$ ground states are populated, such that $\chi_M T$ is close to the value expected for free ions, but as the temperature decreases, a progressive depopulation of higher Stark levels occurs, so the value of $\chi_M T$ begins to decrease. This phenomenon was also observed in other compounds containing Ce^{3+} ions.[35]

A similar evolution is observed in the case of **2**. For **2**, the $\chi_M T$ value at 300 K is 7.01 emu K mol^{-1} (7.49 μ_B), which is lower than the expected value 8.20 emu K mol^{-1} (8.10 μ_B, considering $g = 8/11$) of five isolated Nd^{3+} ions in the $^4I_{9/2}$ ground state. When decreasing the temperature, $\chi_M T$ products of **2** decrease monotonically to the minimum of 3.35 emu K mol^{-1} at 2 K. The whole profile of $\chi_M T$ versus T is similar to those previous reported mononuclear and homodinuclear Nd^{3+} compounds.[36] In the high temperature range of 50−300 K, the magnetic susceptibility of **2** obeys the Curie−Weiss law. Curve fits for $1/\chi_M$ versus T plots of **2** with the Curie−Weiss law in the range 50−300 K afford $C = 7.91$ emu K mol^{-1} and $\theta = -39.63$ K. The deviation of the magnetic susceptibility with respect to the Curie law is due to the crystal field which splits the $^4I_{9/2}$ free-ion ground state into five Kramers doublets. These doublets are almost equally populated at 300 K, such that $\chi_M T$ is close to the value calculated. As the temperature decreases, the Kramers doublets of higher energy are progressively depopulated, so the value of $\chi_M T$ begins to decrease. Finally, the nature of the interactions between the two Nd(III) ions with an orbital momentum cannot be unambiguously deduced only from the shape of the $\chi_M T$ versus T curve.

For **3** and **4**, their magnetic behaviors are very similar. For **3**, the $\chi_M T$ value at 300 K is 3.23 emu K mol^{-1} (5.08 μ_B), which corresponds well with the expected value of 3.21 emu K mol^{-1} (5.07 μ_B, considering $g = 6/7$) of four isolated Ce^{3+} ions in the $^2F_{5/2}$ ground state. When decreasing the temperature, $\chi_M T$ products of **3** decrease gradually to a minimum of 1.73 emu K mol^{-1} at 2 K. Curve fits for $1/\chi_M$ versus T plots of **3** with Curie−Weiss law in the range of 50−300 K results in $C = 3.46$ emu cm^3 K mol^{-1} and $\theta = -18.42$ K. For **4**, the $\chi_M T$ value at 300 K is 6.64 emu K mol^{-1} (7.29 μ_B), which is slightly higher than the expected value 6.56 emu K mol^{-1} (7.24 μ_B, considering $zg = 8/11$) of four isolated Nd^{3+} ions in the $^4I_{9/2}$ ground state. When decreasing the temperature, $\chi_M T$ products of **4** also decrease gradually to a minimum of 3.35 emu K mol^{-1} at 2 K. The Curie−Weiss law was used to fit $1/\chi_M$ versus T plots above 50 K, giving $C = 7.39$ emu K mol^{-1} and $\theta = -29.46$ K. In **3** and **4**, the decrease of $\chi_M T$ upon

(34) (a) Bunzli, J. C. G.; Chopin, G. R. *Lanthanide probes in Life, Chemical and Earth Sciences*; Elsevier: Amsterdam, The Netherlands, 1989. (b) Costes, J. P.; Nicodème, F. *Chem.—Eur. J.* **2002**, *8*, 3442. (c) Benelli, C.; Gatteschi, D. *Chem. Rev.* **2002**, *102*, 2369.

(35) (a) Panagiotopoulos, A.; Zafiropoulos, T. F.; Perlepes, S. P.; Bakalbassis, E.; Masson-Ramade, I.; Kahn, O.; Terzis, A.; Raptopoulou, C. P. *Inorg. Chem.* **1995**, *34*, 4918. (b) Abbas, G.; Lan, Y. H.; Kostakis, G.; Anson, C. E.; Powell, A. K. *Inorg. Chim. Acta* **2008**, *361*, 3494.

(36) (a) Andruh, M.; Bakalbassis, E.; Kahn, O.; Trombe, J. C.; Porcher, P. *Inorg. Chem.* **1993**, *32*, 1616. (b) Hou, H. W.; Li, G.; Li, L. K.; Zhu, Y.; Meng, X. R.; Fan, Y. T. *Inorg. Chem.* **2003**, *42*, 428.

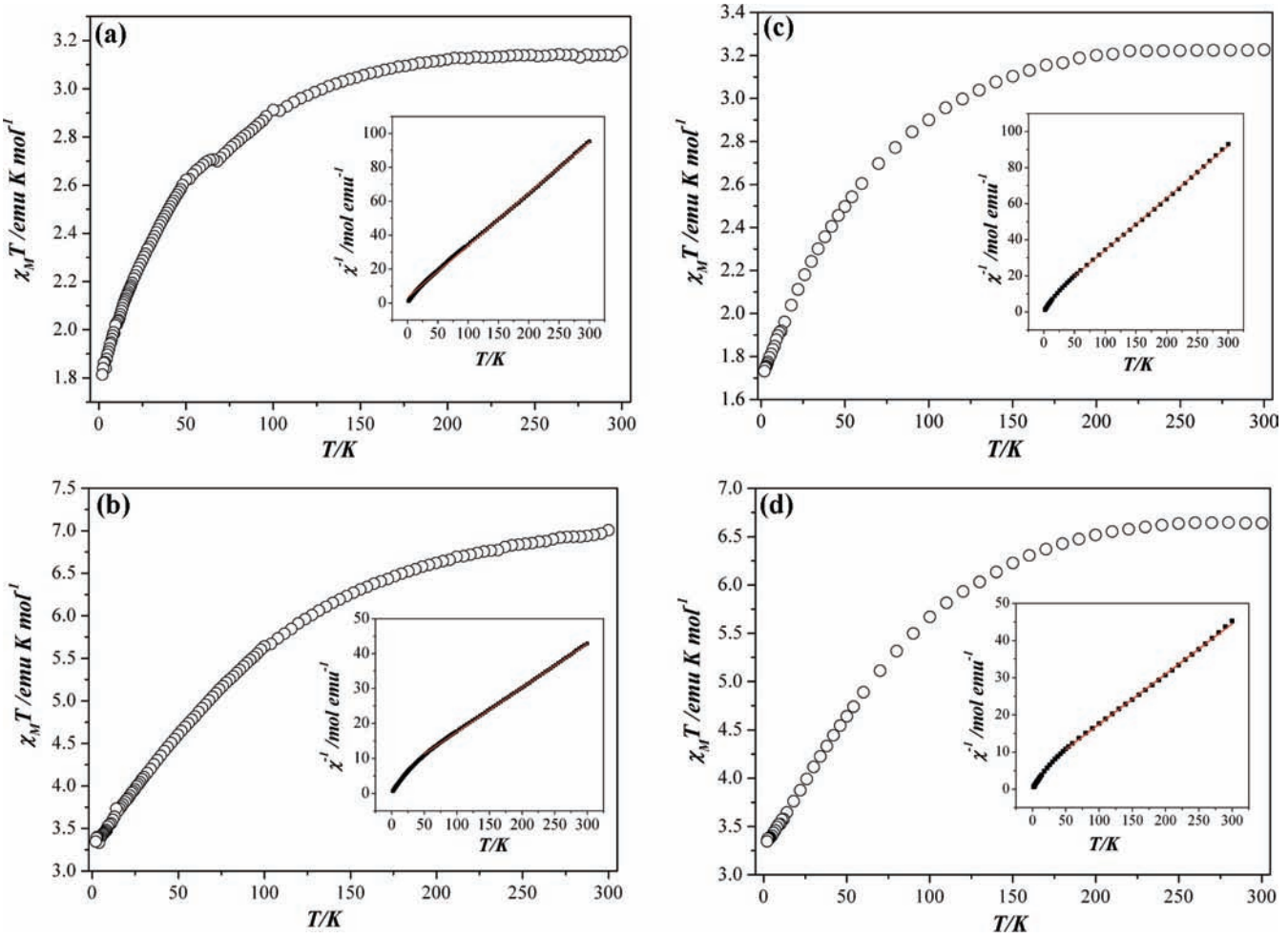

Figure 9. (a) Temperature dependence of reciprocal magnetic susceptibility $\chi_M{}^{-1}$ (square) and the product $\chi_M T$ (circle) for compound **1**. (a) The temperature dependence of reciprocal magnetic susceptibility $\chi_M{}^{-1}$ (square) and the product $\chi_M T$ (circle) for compound **2**. (c) The temperature dependence of reciprocal magnetic susceptibility $\chi_M{}^{-1}$ (square) and the product $\chi_M T$ (circle) for compound **3**. (d) The temperature dependence of reciprocal magnetic susceptibility $\chi_M{}^{-1}$ (square) and the product $\chi_M T$ (circle) for compound **4**.

lowering of the temperature is also governed by depopulation of the Ln^{3+} Stark levels. Similar trends have also been observed in other lanthanide POMs or lanthanide coordination complexes.[37]

Photoluminescence Properties of Compounds 5 and 6. We have measured the photoluminescence spectrum of powder samples of compounds **5** and **6** at room temperature, as shown in Figure 10 and Supporting Information, Figure S10. The results of photoluminescence measurements reveal that **5** shows the characteristic emission bands of the Eu^{3+} ions and weak ligand-based emission band at 439 nm. However, compound **6** shows predominant ligand-based emission at 438 nm, probably caused by the fact that the lowest triplet state energy level of the ligand does not match well to the resonance level of the Sm^{3+} ions, according to the literature.[31]

When the europium compound **5** was measured under excitation at 396 nm, the compound exhibits red photoluminescence. The emission bands at 552, 589, 613, 649, and 696 nm correspond to the $^5D_0$-$^7F_0$, $^5D_0$-$^7F_1$, $^5D_0$-$^7F_2$, $^5D_0$-$^7F_3$, and $^5D_0$-$^7F_4$ transitions, respectively. As we know, the $^5D_0$-$^7F_0$ transition is strictly forbidden by symmetry. The presence of the weak symmetry forbidden $^5D_0$-$^7F_0$ transition at 552 nm indicates that the Eu(III) ions occupy low-symmetry coordination sites with no inversion centers,

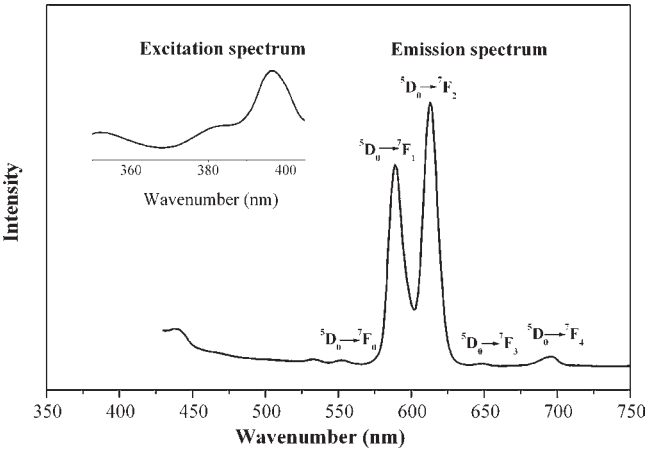

Figure 10. Solid-state photoluminescence spectrum of compound **5** at room temperature.

(37) (a) Hu, M. X.; Chen, Y. G.; Zhang, C. J.; Kong, Q. J. *CrystEngComm* **2010**, *12*, 1454. (b) Liu, L. Z.; Li, F. Y.; Xu, L.; Liu, X. Z.; Gao, G. G. *J. Solid State Chem.* **2010**, *183*, 350. (c) Li, Y.; Zheng, F. K.; Liu, X.; Zou, W. Q.; Guo, G. C.; Lu, C. Z.; Huang, J. S. *Inorg. Chem.* **2006**, *45*, 6308.

in agreement with the result of X-ray structural analysis. The $^5D_0$-$^7F_1$ transition at 589 nm is a magnetic-dipole transition, and its intensity varies with the ligand field strength acting on the Eu^{3+} ion. The $^5D_0$-$^7F_2$ transition at 613 nm is an electric-dipole transition and is extremely sensitive to chemical bonds in the vicinity of the Eu^{3+} ion. Among these transitions, $^5D_0$-$^7F_2$ is the strongest. The intensity of the $^5D_0$-$^7F_2$ transition increases as the site symmetry of the Eu^{3+} ion decreases. So, the intensity ratio of the $I(^5D_0$-$^7F_2)/I(^5D_0$-$^7F_1)$ transition is widely used as a measure of the coordination state and site symmetry of the rare earth ions.[10] For **5**, the intensity ratio $I(^5D_0$-$^7F_2)/I(^5D_0$-$^7F_1)$ is equal to about 1.3, higher than 0.67, a typical value for a centrosymmetric Eu(III) center, which further confirms that Eu(III) ions occupy sites with low symmetry and without an inversion center. In **6**, the absence of the emission of Sm^{3+} ions may be attributed to the large energy difference between the lowest triplet energy level of the ligand and the resonant emissive energy level of Sm^{3+} ions. In addition, coordination of water molecules would generally decrease the photoluminescence intensity of a lanthanide complex because the thermal oscillation of the water molecules consumes some excitation energy absorbed by the "antenna" ligands.

Conclusions

In summary, four novel compounds **1**−**4** constructed from lanthanide-substituted double-Keggin-type polyoxoanions $[\{(H_2O)_4Ln(BW_{11}O_{39}H)\}_2]^{10-}$ and lanthanide cations or lanthanide-organic coordination units have been successfully synthesized, exhibiting 3D open-framework assemblies with 1D channels. The $[\{(H_2O)_4Ln(BW_{11}O_{39}H)\}_2]^{10-}$ as building block is a dimer where the Ln cation is bound to the four oxygen atoms in the cap vacancy of the polyoxoanion and to four water molecules and to a terminal tungsten oxygen. To our best knowledge, compounds **1**−**4** represent the first examples of 3D architectures based on lanthanide-substituted POMs. The 3D frameworks of compounds **1**−**4** are binodal with three- and six-connected nodes and exhibit a rutile topology. The magnetic properties of **1**−**4** have been studied, and the depopulation of the Stark levels in compounds **1**−**4** leads to a continuous decrease in $\chi_M T$ when the samples are cooled from 300 to 2 K. The success in synthesizing compounds **1**−**4** not only provides innovative examples in the realm of 3D POMs, but also may open up possibilities for the design of other 3D LSP-based materials with particular functions. In addition, the structural variation from the 3D open frameworks in **3** and **4** to the 3D supramolecular channel networks in **5** and **6** demonstrates that the lanthanide contraction effect can play a prominent directing role in the architecture of POMs-based hybrid frameworks, and the dimensionalities of these compounds are dependent on the nature of the lanthanide cations.

Acknowledgment. The authors thank the National Natural Science Foundation of China (20901013), Specialized Research Fund for the Doctoral Program of Higher Education (200801411012), Scientific Research Foundation for Doctor of Liaoning Province of China (20081092), the Science Foundation and the Young Teachers' Training Foundation of Dalian University of Technology for financial supports.

Supporting Information Available: Further details are given in Tables S1−S4 and Figures S1−S10. This material is available free of charge via the Internet at http://pubs.acs.org.